SSCL-Preprint-33

Superconducting Super Collider Laboratory

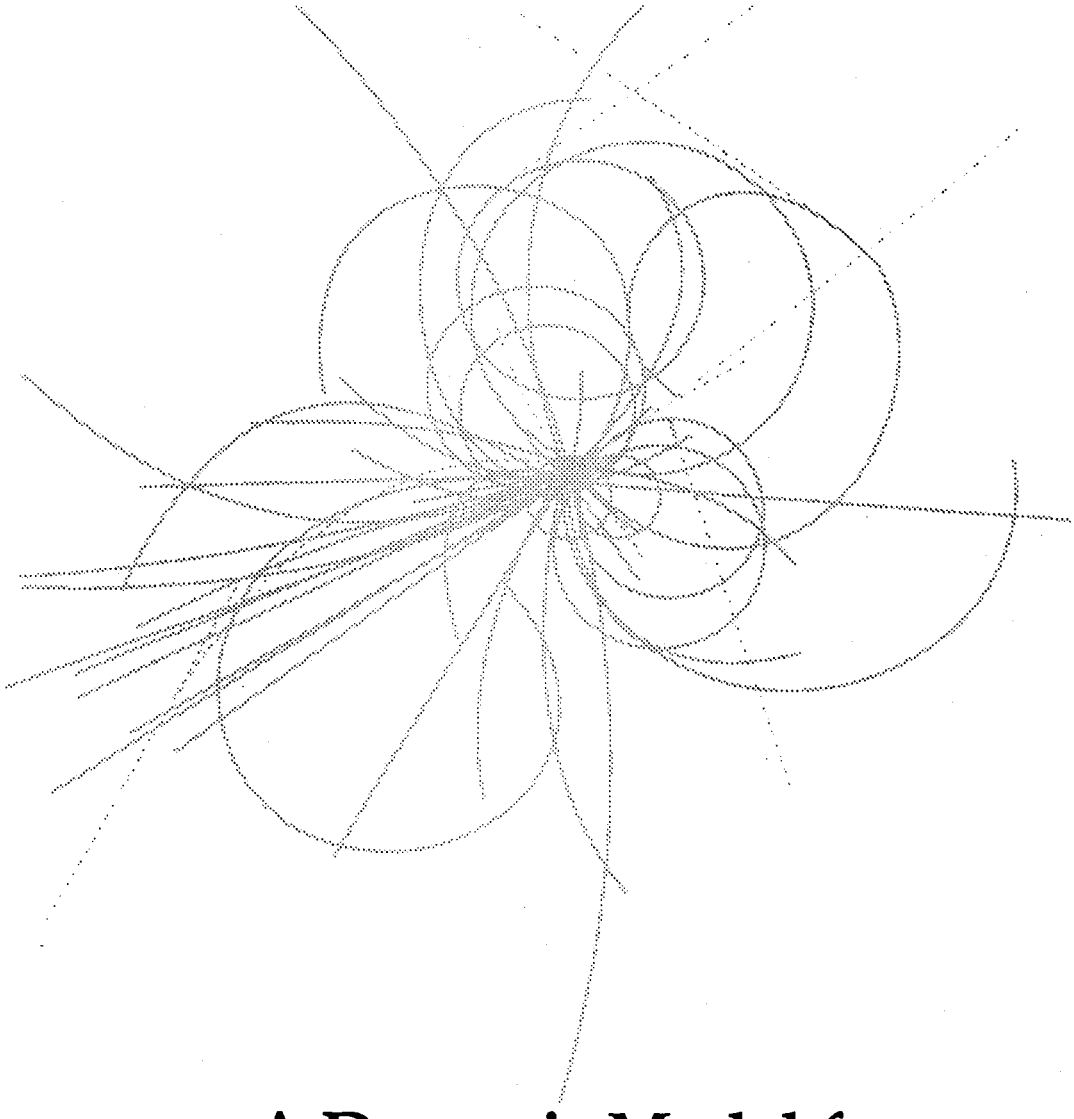

A Dynamic Model for Beam Tube Vacuum Effects on the SSC Cryogenic System

R. H. Carcagno, W. E. Schiesser,
H.–J. Shih, X. Xu, and A. Yücel

March 1992

To be published in *Supercollider 4*

SSCL-Preprint-33

A Dynamic Model for Beam Tube Vacuum Effects on the SSC Cryogenic System*

R. H. Carcagno, W. E. Schiesser, H.-J. Shih, X. Xu, and A. Yücel

Superconducting Super Collider Laboratory†
2550 Beckleymeade Avenue
Dallas, Texas 75237

March 1992

*Presented at the International Industrial Symposium on the Super Collider, New Orleans, March 4–6, 1992.

†Operated by the Universities Research Association, Inc., for the U.S. Department of Energy under Contract No. DE-AC35-89ER40486.

A DYNAMIC MODEL FOR BEAM TUBE VACUUM EFFECTS ON THE SSC CRYOGENIC SYSTEM

R. H. Carcagno, W. E. Schiesser, H.-J. Shih, X. Xu, and A. Yücel

Superconducting Super Collider Laboratory*
2550 Beckleymeade Ave.
Dallas, TX 75237

Abstract: The dynamic interaction between the beam-gas scattering induced energy deposition and the SSC cryogenic system is studied by integrating a cryogenic system dynamic simulator with an adsorption model and a beam-gas scattering and energy deposition model. Simulation results are obtained for a 1 km long SSC arc section where the beam tube pressure in one of the dipoles is increased up to 150 times its nominal operating pressure. The beam-gas scattering induced heat loads arising from such high pressure perturbations can be very high locally but do not overload the cryogenic system. They are more likely to induce a magnet quench as they result in coil temperatures that largely exceed the desired operating limit. Simulations are also carried out for the case where a large external heat load of 1 W/m is imposed on the coldmass of a half-cell in the section. Results show that the coldmass temperatures rise significantly with the added heat load but the energy deposition in the coldmass due to beam-gas scattering remains low despite the increase in the beam tube temperature.

1.0 INTRODUCTION

It has been noted that a local disturbance in the SSC beam tube pressure would initiate a process that may eventually make it necessary to shut down the collider due to a local overload of the cryogenic system before any effect is seen on the beam lifetime. In the SSC baseline design, the beam tube vacuum is maintained at a nominal pressure level of 1.3×10^{-10} torr and the beam tube at 4.17 K. During the operation of the collider, synchrotron light photons continuously strike the beam tube surface and release H_2 molecules and other gases. The gas molecules are pumped or adsorbed by the cold beam tube surface, but are re-desorbed easily by the flux of photons. The resulting density of gas molecules in the beam tube scatters the protons in the beam, which not only reduces the beam lifetime, but also produces particle showers which deposit energy in the coldmass [1].

In the event that the beam-tube vacuum is degraded at a small section such as one dipole, the increased density of H_2 molecules will yield increased energy deposition in the coldmass, causing the coldmass temperature to rise. As the beam tube temperature increases, the gas equilibrium pressure and consequently the gas density increases, which further raises the beam-gas heat load on the

* Operated by the Universities Research Association, Inc. for the U.S. Department of Energy under Contract No. DE-AC35-89ER40486.

Radial range (cm)	Material
0. - 1.64	vacuum
1.64 - 1.85	bore tube (Fe)
1.85 - 2.50	liquid helium
2.50 - 3.70	inner coil (NbTi & Cu)
3.70 - 5.00	outer coil (NbTi & Cu)
5.00 - 6.80	collar (Fe)
6.80 - 16.4	yoke (Fe)

Table 1: Dipole Radial Configuration

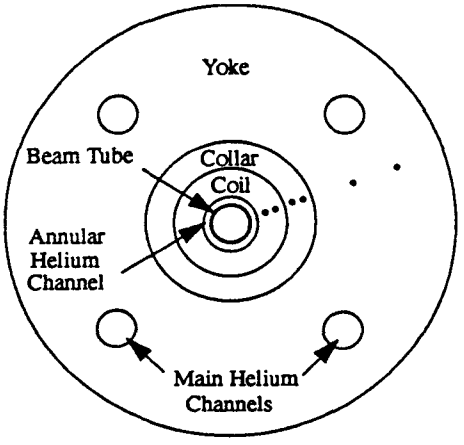

Figure 1. Schematic of the coldmass assembly

cryogenic system. If the cryogenic system can not maintain the beam tube temperature below a certain level, the above mentioned phenomenon could continue and cause the collider to shut down.

The purpose of this work is to analyze this phenomenon and evaluate its potential effect on the cryogenic system operation. Three models have been integrated: the beam-gas interaction model provides the energy deposition for each proton-proton collision resulting from beam-gas interactions each second at every meter of the magnet; the adsorption model provides the density of the hydrogen molecules available to collide with the proton beam; and the cryogenic system dynamic simulator simulates the cryogenic system response to the total energy deposition for a given section of the magnet string, obtained from the other two models.

An increased heat load on the coldmass due to a source other than the beam tube vacuum degradation can also raise the temperature of the coldmass and the beam tube, and trigger the above described phenomenon. Therefore, in addition to the problem of a local perturbation in the beam tube pressure, we also analyzed the problem of a perturbation in the external heat input to the coldmass.

2.0 BEAM-GAS INTERACTION INDUCED ENERGY DEPOSITION MODEL

This section describes the simulation of energy deposition in a regular half cell due to beam-gas collisions. Protons in the circulating beams interact with the gas in the beam pipe. Most of the particles produced in beam-gas collisions enter and interact with matter in the magnets, creating cascades of particles and depositing energy. Since the predominant gas is hydrogen in the cold section, beam-gas collisions are in effect proton-proton collisions.

Particle production in proton-proton collisions is simulated using the Monte-Carlo program ISAJET [2]. Five thousand events are generated at the center-of-mass energy of 194 GeV. The collision points are uniformly distributed along a unit length of one meter. Particle cascades and the associated energy deposition in a half cell are simulated using the Monte-Carlo program MARS10 [3]. In the simulation, a half cell consists of 5 dipoles each of length 15.815 meters and a quadrupole of length 5.85 meters. The spool pieces are ignored. The radial configuration of the dipoles are shown in Table 1 and in Fig. 1. Dipoles are curved with a bending angle of 0.086 degrees. The magnetic fields, with strengths of 6.6 Tesla in dipoles and 2.056 Tesla/meter in the quadrupoles, are present only in the vacuum. The superconductors are composed of 62% Cu, 19% Ti and 19% Nb.

Shown in Fig. 2(a) are the energy depositions per meter in a half cell and in different layers of the magnet for one beam-gas collision (one event). The energy deposition in the helium in the annular channel is negligible. The first peak, about 8 meters downstream, is caused by the charged particles from beam-gas collisions. The second peak is caused by the neutrals and should be near the point where the neutrals hit the beam tube which is about 19 meters downstream according to the geometry, $\sqrt{2xr}$. Here x is the inner radius of the dipole beam tube and r is the dipole radius of curvature.

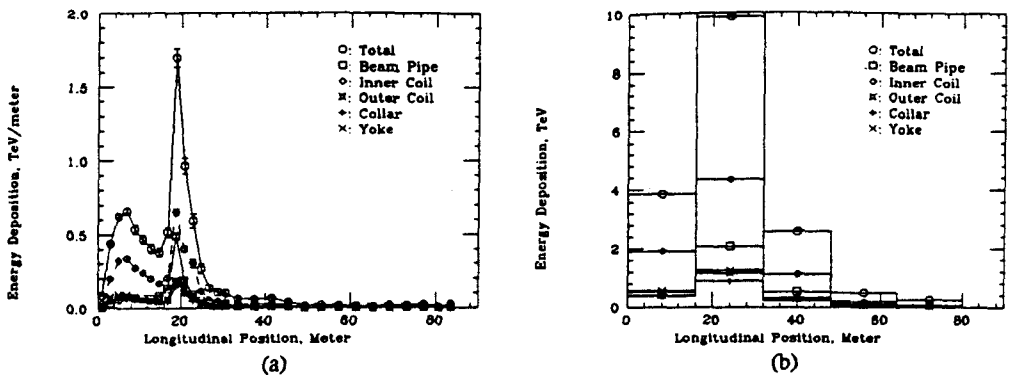

Figure 2. Energy depositions from beam-gas scattering in (a) one event per meter, (b) one event per dipole.

Fig. 2(b) shows the energy depositions per dipole in different layers of the magnet for one beam-gas collision, obtained by integrating Fig. 2(a) over the length of one dipole (15.8 m) and dividing by the length. Since we consider one dipole as the basic unit, the values in this figure are used in our model.

3.0 ADSORPTION MODEL

From the beam-gas interaction model, we are able to obtain the amount of energy released from a single event in one dipole. In this section, we will develop a model that calculates the number density of H_2 gas molecules in the beam pipe, ρ, as a function of the beam pipe pressure and temperature. The number density will then be used to determine the number of collisions and consequently, the total energy deposition from beam-gas scattering.

The adsorption model is based on the BET equation for the physical adsorption process [4]. Consider a beam tube of diameter D and length L. For a given temperature T and pressure P, the total number of molecules in the tube, N_t, can be written as

$$N_t = N_a + N_v, \tag{1}$$

where N_a is the number of adsorbed molecules, and N_v the number of gas molecules.

N_a is given by the BET equation:

$$N_a = \pi D L n_m \frac{zx}{(1-x)\,[1+(z-1)x]}, \tag{2}$$

where $x = P/P_{sat}$, $z = e^{\theta/T}$, n_m is the number of molecules in a monolayer per unit area, and θ is related to the energy of adsorption. The gas adsorption parameters n_m and θ are determined from experiments. For hydrogen gas with stainless steel, we have estimated the following values based on the experiments of Benvenuti et al. [5]:

$n_m = 0.66 \times 10^{16}\ \mathrm{cm}^{-2}$, θ = 41 K.

The saturation pressure is given by:

$$ln(P_{sat}) = 4.7222 - 90.593/T + 2.1269 ln(T), \tag{3}$$

and N_v is given by the ideal gas equation:

$$N_v = \frac{\pi D^2}{4} L \frac{P}{kT}, \tag{4}$$

where k is the Boltzmann constant.

During a transient, as the beam-tube and the gas temperatures increase due to increased heat load, the relative compositions of adsorbed vs. gas molecules will be affected while the total number of molecules, N_t, remains unchanged. Under the quasi-equilibrium process assumption, the new equilibrium pressure P' corresponding to temperature T' at a given instant is:

$$P' = x' P_{sat}(T') \,, \tag{5}$$

where x' is obtained by solving the equation: $N_t = N_t' = N_a(x', T') + N_v(x', T')$.

The number density of H_2 gas molecules (molecules/m^3), ρ, is subsequently calculated from

$$\rho = \frac{N_v}{(\pi L D^2/4)} = \frac{P}{kT}. \tag{6}$$

The number of interactions per second per meter, N_{int}, can be computed from

$$N_{int} = 2\rho\sigma N_{beam} f_{rot}, \tag{7}$$

where σ is the proton-proton scattering cross-section (5×10^{-30} cm^2), N_{beam} is the number of protons per beam (1.3×10^{14}), and f_{rot} is the rotation frequency of the beam (3.44 kHz).

The heat deposition due to beam-gas interactions is proportional to the number of beam-gas interactions and is given by:

$$q_{bg} = E_{1event} \times N_{int}, \tag{8}$$

where E_{1event} is the beam-gas scattering energy distribution from a single event, given by the beam-gas model.

4.0 SSCDYSIM, v2.0

4.1 The SSC Cryogenic System

The SSC requires an extensive cryogenic system that not only accommodates the operating conditions of the superconducting magnets, but also the transient conditions such as cooldown, beam acceleration, magnet quench and magnet maintenance. The SSC cryogenic system contains twelve equal sized helium refrigeration plants, ten for the collider and two for the high energy booster. Each plant on the collider provides cooling for a 8.6-km sector of both rings. A more detailed description of the cryogenic sector structure can be found in reference 6.

Fig. 3 illustrates the flow diagram of the cryogenic system for a portion of the collider rings. Single-phase helium at 4.15K and 4 atm from a refrigeration plant is pumped into the magnet strings. It flows through the magnets in series and is recooled at intervals of one cell to maintain the magnets below 4.35 K. Encompassing these pipes are the 20K and 84K shields with multilayer insu-

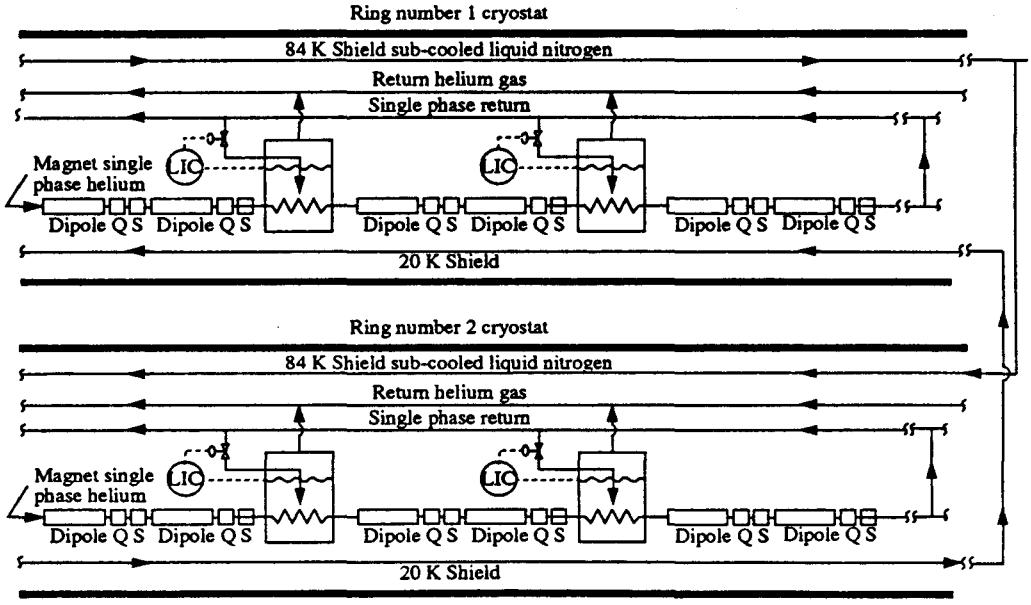

Figure 3. The flow diagram of the SSC cryogenic system

lation, and all these are contained in a vacuum vessel to form the cryostat.

4.2 The Flexible Flowsheet Dynamic Process Simulator, SSCDYSIM, v2.0

To study the operation of the SSC cryogenic system under various transient conditions, the SSC Central Design group and Air Products and Chemicals, Inc. have developed a dynamic process simulator, SSCDYSIM, v1.0 [7]. This dynamic process simulator is based on a nonlinear, homogeneous, lumped-parameter physical model. It is written in FORTRAN, and has a modular structure. It uses the LSODES [8] integration package, and incorporates Air Products' implementation of the NBS helium thermodynamic model and two additional simplified models for the helium properties.

Since SSCDYSIM, v1.0 is a fixed-flowsheet simulator, it is difficult to make modifications when a new problem is to be studied and a new flowsheet is to be built. Thus, we have upgraded version 1.0 to make version 2.0 a flexible-flowsheet simulator.

Unlike version 1.0, a flowsheet for SSCDYSIM v2.0 can be built with a small set of object types and connection types, and it is easy to add or remove objects from the flowsheet without changing the source code. The structure of SSCDYSIM v2.0 also allows for easy addition of new object types and/or connection types. The majority of the code in SSCDYSIM v2.0 was written in C programming language, except the LSODES integration package and the Air Products' helium property package.

SSCDYSIM v2.0 uses the C facility "structure" to represent each type of object, such as volume, recooler, pump, valve, etc. This is similar to the convention of lumped-nodes in SSCDYSIM v1.0. The flows between these objects are called "streams". Any physically feasible connection between two objects can easily be accomplished through these streams. Adding or deleting the objects therefore is very convenient.

In addition to simulating the process flow, SSCDYSIM v2.0 also has the capability of solving heat transfer problems such as conduction, convection, and radiation. Hence, the heat transfer problems in the magnets can be coupled with the process flow of the cryogenic system.

5.0 MODELING PROCEDURE

To study the effect of beam-gas scattering energy deposition on the SSC cryogenic system, we have integrated the beam-gas interaction model and the adsorption model into the cryogenic process simulator. Based on the two-dimensional energy distribution from the beam-gas model and the number density of the H_2 gas molecules, we can calculate from Eq. (8) the energy deposition for all the beam-gas collisions. Taking this energy deposition as the dynamic heat load to a dipole in our SSCDYSIM flowsheet, we can solve various process flow problems and calculate the response of the cryogenic system to that heat load, such as the variations in recooler duty, the helium pressure and temperature in the magnets, and in the liquid return and vapor return lines.

The study was conducted on one section of one string, about 1 km long, as shown in Fig. 4. The section has 6 cells, and each cell has 10 dipoles. The helium in the main channels of each dipole is lumped into one node and is represented by a dot in Fig. 4. The coldmass configuration is shown in Fig. 1. As shown in Fig. 1, we used 6 nodes in the coldmass of each dipole to account for heat conduction; the coil, collar and yoke each has 2 nodes. The energy deposition in each layer (Fig. 2)

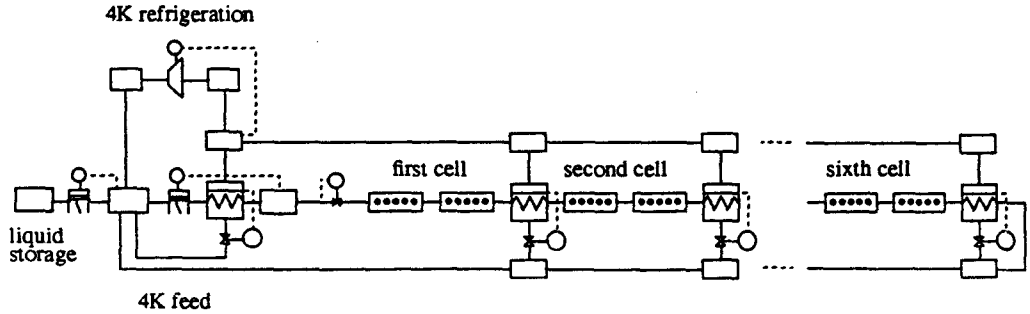

Figure 4. The flowsheet for the beam-tube vacuum adsorption study

is assigned to the corresponding node.

The current flowsheet does not include any nodes for the beam tube and for the helium in the annular channel. Thus, the effects of convection in the annular channel are not accounted for. Therefore, the synchrotron radiation load and the beam-gas load to the beam tube are allocated directly to the inner coil node. In order to obtain the beam tube inner surface temperature to be used in the adsorption model, we have developed a separate three-dimensional model to solve for the detailed heat transfer problem in the coldmass, including the axial flow in the annular helium channel along a 15.8 m dipole. Using this model, the beam-tube temperature along a dipole can be calculated given the heat load distribution and the temperature of the helium in the main cooling channel. To this end, we have used an iterative procedure outlined below:

- For a given heat load, apply the simulator to solve for the helium temperature in the main channel.
- Use the thermal resistances obtained from the detailed heat transfer model to compute the beam-tube surface temperature. To be conservative, we have used the temperature distributions at the end of the dipole, where the beam-tube temperature is higher and hence renders higher beam-gas load.
- Calculate the beam-gas heat load from this beam-tube temperature and supply the load into the simulator which in turn gives new helium temperature in the main channel.

As a first step in the simulation, we obtained the steady state condition under the nominal static heat load and dynamic heat load (including synchrotron radiation load and beam-gas scattering at $P=1.3\times10^{-10}$ torr). We then impose a perturbation in the beam-pipe pressure or a perturbation in the external heat input. Two scenarios were considered: a) a local beam-tube pressure bump in a dipole, and b) a local heat load disturbance in a half cell.

6.0 DISCUSSION OF RESULTS

6.1 Beam Tube Vacuum Degradation in a Dipole

As shown in Fig. 4, the degradation in beam-tube vacuum is assumed to occur at the ninth dipole of the second cell where the overall temperature here is the second highest in the cell. Most of the scattering energy is deposited in the next dipole, which constitutes the worst case scenario. After running in steady state for 10 minutes, we perturbed the beam-pipe pressure in one dipole and obtained the results for a range of test conditions.

Figs. 5(a)-(b) show the temperature profiles in the helium channel and in the inner coil along the 1 km long string section at different times, with the pressure bump being 150 times the nominal value of $\sim3\times10^{-10}$ torr. It can be seen from Figs. 5(a)-(b) that this pressure bump causes only a moderate increase in the helium temperature (~110 mK), but a relatively large increase in the inner coil temperature (~420 mK) in the tenth dipole. This is somewhat obvious by examining Fig. 2(b). Most of the beam-gas scattering energy is deposited in the second dipole, and radially, about half of the

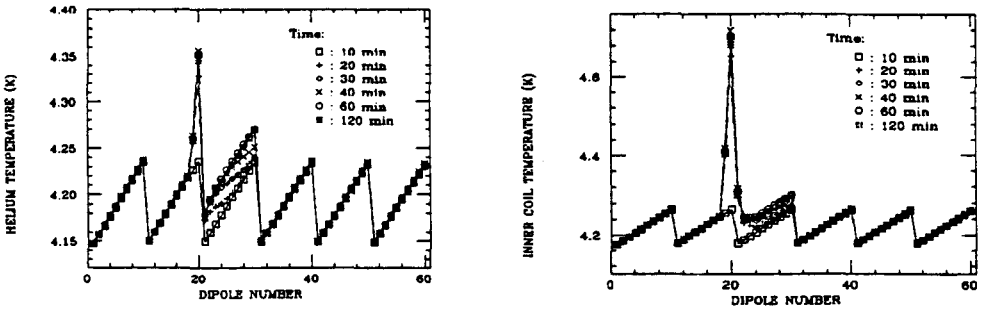

(a) (b)

Figure 5. Temperature profiles along the 1 km section for 150 fold pressure bump: (a) helium, (b) inner coil.

total energy is deposited in the inner coil.

Figs. 5(a)-(b) also show that the pressure bump effect is confined to the second and the third cells. The beam-gas scattering heat load is far less than the recooler capacity, and the temperatures of the dipoles in the fourth cell remain unchanged. The heat duties of the second and the third cell recoolers are 78 W and 51 W respectively, up from the nominal value of 39 W.

While the cryogenic system capacity is not exceeded for such a high pressure perturbation, the inner coil temperature of the tenth dipole in the second cell ($T \approx 4.68$ K) is far above the desired operating limit of 4.35 K. Therefore, the increased heat load due to beam tube vacuum degradation in a dipole is more likely to initiate a magnet quench before levels that would overload the cryogenic system can be attained. We also studied cases with beam tube pressure perturbations of 100 and 50 times the nominal value: the corresponding inner coil temperatures for the tenth dipole are 4.44 K and 4.33 K.

6.2 Heat Load Disturbance in a Half-Cell

The effect of an sudden increase in the heat load of a half cell due to an external source was studied. As before, after 10 minutes of steady state operation, an additional heat load of 1 W/m was imposed on the first half-cell of the second cell. This load is assumed to originate from outside the coldmass (e.g. due to a leak in the cryostat insulating vacuum) and is therefore assigned to the outer layer of the yoke in the model.

Fig. 6(a)-(b) depict the resulting temperature profiles along the 1 km long string section at different times. The largest temperature increases occur in the last dipole (about 220 mK for the helium and 240 mK for the inner coil). Despite the increased beam tube temperature levels in the second cell, the corresponding gas equilibrium pressures in the beam tube do not reach the levels to produce significant beam-gas scattering effects. The recooler duty for the second cell increases to 119 W as a result of the added external heat load. The effects of the disturbance are localized, resulting slightly higher temperatures in the next cell and a small increase (from 39 W to 43 W) in the recooler duty for the next cell.

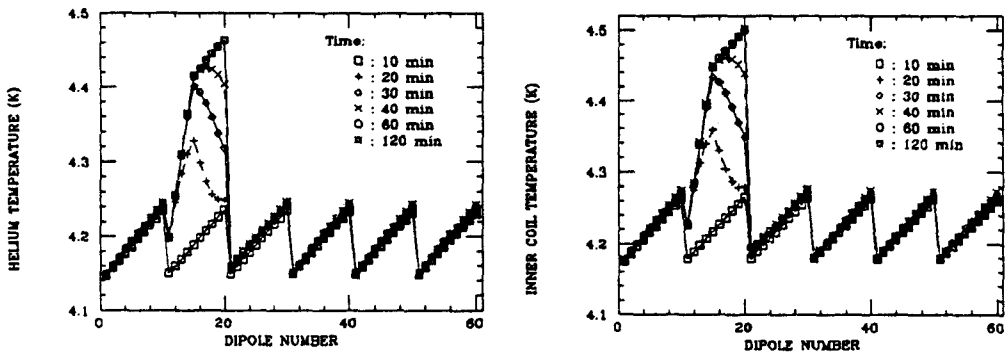

Figure 6. Temperature profiles along the 1 km section for the heat load perturbation of 1W/m: (a) helium, (b) inner coil.

7.0 CONCLUSIONS

We have studied the dynamic interaction between the beam-gas scattering energy deposition and the SSC cryogenic system by integrating a cryogenic system dynamic simulator with an adsorption model and a beam-gas scattering and energy deposition model. We have obtained simulation results for one SSC string section that shows the cryogenic system evolving toward new states as a result of a) a local disturbance in the beam-tube pressure in a dipole, and b) a local disturbance in the heat load of a half-cell.

In the case of a perturbation in the beam tube pressure of a dipole, the cryogenic system capacity can easily accommodate the increased energy deposition in the coldmass due to beam-gas scattering. The beam-gas scattering effect does not propagate than the following cell. The beam-gas scattering has a more immediate impact on the coil temperature than on the cryogenic system capacity and can provoke a magnet quench for a sufficiently high perturbation in the beam-tube pressure. In the case of an externally imposed heat load on a half-cell, the beam-gas scattering induced energy deposition remains low despite high beam tube temperatures.

8.0 REFERENCES

1. Edwards, H.T., "Study on Beam Tube Vacuum with Consideration of Synchrotron Light, Potential Liner Intercept, and Collider Quad/Spool Coil Diameter," *SSC Report SSCL-N-771*, August, 1991.
2. Paige, F.E., and Protopopescu, S.D., "ISAJET 6.24: A Monte Carlo Event Generator for p-p and pbar-p Reactions," *BNL Document*, 1990.
3. Mokhov, N.V., "The MARS10 Code System: Inclusive Simulation of Hadronic and Electronmagnetic Cascades and Muon Transport," *Fermilab Report FN-509*, March 20, 1989.
4. Brunauer, S., Emmett, P.H., and Teller., E., "BET Model for Physical Adsorption," *J. Am. Chem. Soc.*, Vol. 60. p 309. 1938.
5. Benvenuti, C., Calder, R.S., and Passardi, G., "Influence of Thermal Radiation on the Vapor Pressure of Condensed Hydrogen (and isotopes) between 2 and 4.5 K," *J. Vac. Sci. Technol.*, Vol. 13, No. 6, Nov/Dec 1976.
6. *Site-Specific Conceptual Design of the Superconducting Super Collider, SSCL-SR-1056*, July, 1990.
7. Hartzog, D.G., et. al., "Dynamic Modeling and Simulation of the Superconducting Super Collider Cryogenic Helium System," *Supercollider 1*, Plenum Press, New York, 1989.
8. Hindmarsh, A.C., "ODEPACK, A Systematized Collection of ODE Solvers," *Scientific Computing*, R.S. Stepleman et al. eds., North-Holland, Amsterdam 1983, pp. 55-64.